REVIEW SUMMARY

PLANAR OPTICS

Metalenses: Versatile multifunctional photonic components

Mohammadreza Khorasaninejad and Federico Capasso*

BACKGROUND: Future high-performance portable and wearable optical devices and systems with small footprints and low weights will require components with small form factors and enhanced functionality. Planar components based on diffractive optics (e.g., gratings, Fresnel lenses) and thin-film optics (e.g., dielectric filters, Bragg reflectors) have been around for decades; however, their limited functionality and difficulty of integration have been key incentives to search for better alternatives. Owing to its potential for vertical integration and marked design flexibility, metasurface-based flat optics provides a rare opportunity to overcome these challenges. The building blocks (BBs) of metasurfaces are subwavelength-spaced scatterers. By suitably adjusting their shape, size, position, and orientation with high spatial resolution, one can control the basic properties of light (phase, amplitude, polarization) and thus engineer its wavefront at will. This possibility greatly expands the frontiers of optical design by enabling multifunctional components with attendant reduction of thickness, size, and complexity.

ADVANCES: Recent progress in fabrication techniques and in the theory and design of metasurfaces holds promise for this new optical platform (metaoptics) to replace or complement conventional components in many applications. One major advance has been the migration to all-dielectric metasurfaces. Here, we discuss the key advantages of using dielectric phase-shifting elements with low optical loss and strong light confinement in the visible and near-infrared regions as BBs of flat lenses (metalenses). High–numerical aperture metalenses that are free of spherical aberrations have been implemented to achieve diffraction-limited focusing with subwavelength resolution, without requiring the complex shapes of aspherical lenses. Achromatic metalenses at discrete wavelengths and over a bandwidth have been realized by dispersion engineering of the phase shifters. By suitably adjusting the geometrical parameters of the latter, one can impart polarization- and wavelength-dependent phases to realize multifunctional metalenses with only one ultrathin layer. For example, polarization-sensitive flat lenses for chiral imaging and circular dichroism spectroscopy with high resolution have been realized, and off-axis metalenses with large engineered angular dispersion have been used to demonstrate miniature spectrometers. The fabrication of metalenses is straightforward and often requires one-step lithography, which can be based on high-throughput techniques such as deep-ultraviolet and nanoimprint lithography.

OUTLOOK: In the near future, the ability to fabricate metalenses and other metaoptical components with a planar process using the same lithographic tools for manufacturing integrated circuits (ICs) will have far-reaching implications. We envision that camera modules widely employed in cell phones, laptops, and myriad applications will become thinner and easier to optically align and package, with metalenses and the complementary metal-oxide semiconductor–compatible sensor manufactured by the same foundries. The unprecedented design freedom of metalenses and other metasurface optical components will greatly expand the range of applications of micro-optics and integrated optics. We foresee a rapidly increasing density of nanoscale optical elements on metasurface-based chips, with attendant marked increases in performance and number of functionalities. Such digital optics will probably follow a Moore-like law, similar to that governing the scaling of ICs, leading to a wide range of high-volume applications. ■

ON OUR WEBSITE

Read the full article at http://dx.doi.org/10.1126/science.aam8100

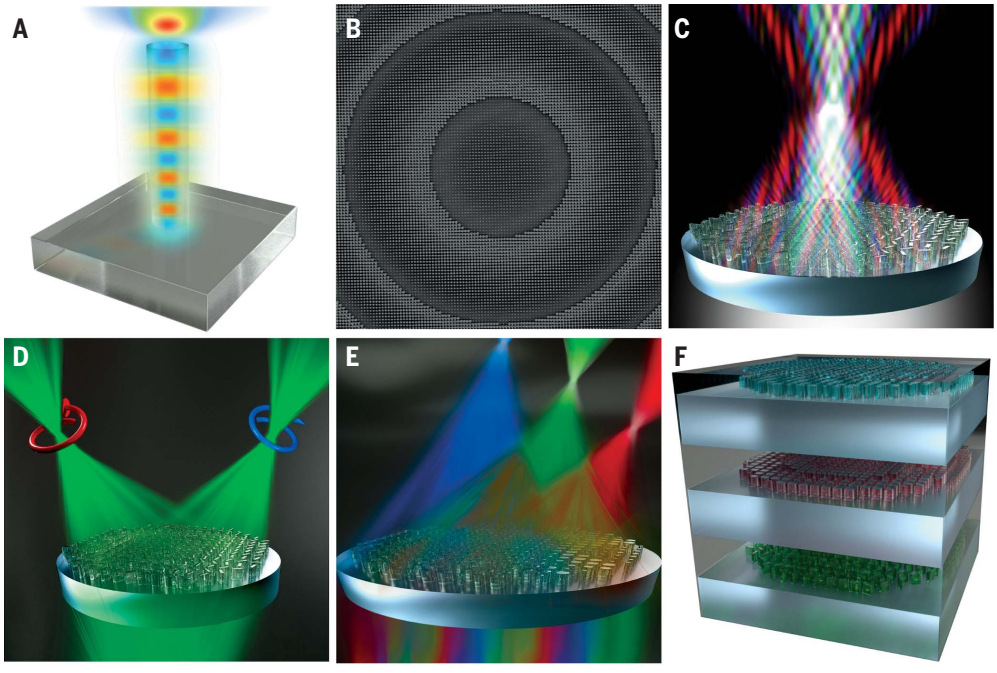

All-dielectric metalenses. (**A**) Schematic of a dielectric pillar acting as a truncated waveguide for phase-shifting the incident light. (**B**) Top-view scanning electron microscopy image of a metalens based on titanium dioxide, with dielectric pillars as BBs. (**C**) Schematic of an achromatic metalens realized by engineering the dispersive response of its BBs. (**D**) Schematic of a chiral metalens that spatially separates and focuses light with different helicities. (**E**) Schematic of a metalens that simultaneously focuses and disperses the incident light. (**F**) Illustration of the concept of vertically stacking metasurfaces to build miniaturized multifunctional systems.

ILLUSTRATIONS: RYAN ALLEN/SECOND BAY STUDIOS

The list of author affiliations is available in the full article online.
*Corresponding author. Email: capasso@seas.harvard.edu
Cite this article as M. Khorasaninejad, F. Capasso, *Science* **358**, eaam8100 (2017).
DOI: 10.1126/science.aam8100

REVIEW

PLANAR OPTICS

Metalenses: Versatile multifunctional photonic components

Mohammadreza Khorasaninejad* **and Federico Capasso†**

Recent progress in metasurface designs fueled by advanced-fabrication techniques has led to the realization of ultrathin, lightweight, and flat lenses (metalenses) with unprecedented functionalities. Owing to straightforward fabrication, generally requiring a single-step lithography, and the possibility of vertical integration, these planar lenses can potentially replace or complement their conventional refractive and diffractive counterparts, leading to further miniaturization of high-performance optical devices and systems. Here we provide a brief overview of the evolution of metalenses, with an emphasis on the visible and near-infrared spectrum, and summarize their important features: diffraction-limited focusing, high-quality imaging, and multifunctionalities. We discuss impending challenges, including aberration correction, and also examine current issues and solutions. We conclude by providing an outlook of this technology platform and identifying promising directions for future research.

Metasurfaces (*1*–*5*) are arrays of subwavelength-spaced optical scatterers (metallic or dielectric) at an interface whose primary function is to locally shift the phase of incident light, thus shaping its wavefront in accordance with the spatial distribution of the scatterers. By spatially adjusting the metasurface building block (MBB) geometrical parameters (such as size, shape, and orientation across a surface), one can control the reflected or transmitted wavefront at will. Metasurfaces are conceptually related to the reflect and transmit arrays demonstrated in the millimeter-wave and microwave ranges (*6*, *7*) but with a very distinct difference: subwavelength arrangements of the MBBs. This enables control over the basic properties of light (phase, amplitude, and polarization) with high spatial resolution. In addition, the subwavelength arrangement circumvents the formation of spurious diffraction orders, which generally prevail in conventional diffractive components such as gratings, where the constitutive elements are spaced on a wavelength scale. These spurious orders not only degrade the efficiency of diffractive components but also give rise to undesired effects such as virtual focal spots, halos, and ghost images. It is notable that there are some diffractive components (e.g., blazed gratings) in which subwavelength arrangement has been used. However, what differentiates metasurfaces from these components is their wide range of possible designs, leading to unprecedented functionalities. For instance, one can independently engineer the interaction of MBBs with the electric as well as the magnetic field components of light, leading to complete control of not only the phase, amplitude, and polarization response but also of the local impedance (*8*–*11*). The latter has been used to suppress reflections by impedance matching. This control is not limited to a single wavelength and can be broadband through suitable dispersion engineering of MBBs. Owing to its design flexibility and versatility, metasurface-based optics (metaoptics) provides opportunities to go beyond what is achievable by conventional diffractive optics. In this Review, we concentrate on recent developments of metasurface-based lenses, hereafter interchangeably dubbed "flat lenses" and "metalenses."

Refractive lenses, such as those used in objectives and telescopes, have useful properties but are often bulky, heavy, and costly. Additionally, for their fabrication, these lenses rely on a relatively old technology, molding, based on realizing in an "analog" way the phase profile required for focusing by suitably shaping the lens. Metasurfaces offer an opportunity to overcome these limitations. In particular, with the use of appropriate sampling methods, the lens phase profile can be accurately digitized using MBBs and then implemented with standard lithographic techniques employed in the manufacturing of integrated circuits. The phase profile $\varphi(r)$ of a flat lens for normally incident light of wavelength λ is hyperbolic, which ensures a diffraction-limited spot (*2*)

$$\varphi(r) = -\frac{2\pi}{\lambda}\left(\sqrt{r^2 + f^2} - f\right) \qquad (1)$$

where f is the focal length and r is the radial position. Equation 1 represents the requirement that all rays must arrive in phase at the focus.

In this Review, we begin with a brief historical perspective of wavefront shaping. Starting with the pioneering works in the microwave range, we trace the progress of this effort into the optical domain through diffractive optics. Rapid progress has since been made by using metasurfaces. By introducing a new approach to wavefront shaping, metasurfaces changed the prospects of what is feasible in a compact and planar platform: flat or planar optics. First, we discuss plasmonic flat lenses, in which the MBBs are deep-subwavelength–spaced metallic elements. The low efficiency of these lenses, associated with the high dissipative loss of metals in the visible and near-infrared (NIR) spectra, poses a major hurdle for applications. Overcoming these deficiencies has been the major incentive for the development of all-dielectric metasurfaces. Next, we discuss recent developments in all-dielectric flat lenses: high efficiency, high numerical apertures (NAs), and multifunctional lenses and their applications in miniaturized systems, along with correction of monochromatic and chromatic aberrations. We conclude by gauging the impact of this platform on the field of optics and by identifying future opportunities for science and technology.

In 1948, Kock (*12*) experimentally demonstrated an artificial material composed of metallic antennas embedded in a polystyrene foam host to build lightweight lenses in the microwave range. This concept was later applied to diffractive optics, where a spatially varying effective permittivity was realized by surface patterning (*13*–*18*). Initially, this was accomplished by thickness modulation across a surface [e.g., the use of sawtooth or staircase surface profiles (*13*–*16*)], where the maximum thickness modulation corresponds to a phase delay of 2π—one of the basic principles of diffractive optics. Aside from their fabrication complexity [that is, the requirement of multilayer masking (*14*, *15*)], these diffractive components inherently suffer from low efficiency arising from the shadowing effect (*16*). This effect becomes more severe when light needs to be diffracted into large angles, as in the case of high-NA lenses. Eventually, a more practical approach was developed, in which the effective refractive index is modulated across the surface by adjusting the lateral size of structures (*17*, *18*) instead of their height. Not only does this approach considerably simplify the fabrication process (single-step lithography), it also eliminates the shadowing effect. For instance, we consider the building block (BB) to be a square-shaped dielectric pillar with width W and height H, arranged in a square lattice with the unit cell size $U \times U$. Each unit cell operates as an element where its effective refractive index, $n_{\text{eff}}(W)$, can be modified by adjusting the pillar width W, which controls the confinement of light. The minimum achievable effective refractive index is that of the surrounding medium, generally air ($n = 1$), when there is no pillar. When a pillar fills the entire unit cell ($W = U$), the effective refractive index attains its maximum value equal to n, the bulk index of material. Light traveling through a unit cell (neglecting Fabry-Perot effects) accumulates a phase shift φ

$$\varphi = \frac{2\pi}{\lambda} \times n_{\text{eff}} \times H \qquad (2)$$

Harvard John A. Paulson School of Engineering and Applied Sciences, Harvard University, Cambridge, MA 02138, USA.
*Present address: Magic Leap, Plantation, FL 33322, USA.
†Corresponding author. Email: capasso@seas.harvard.edu

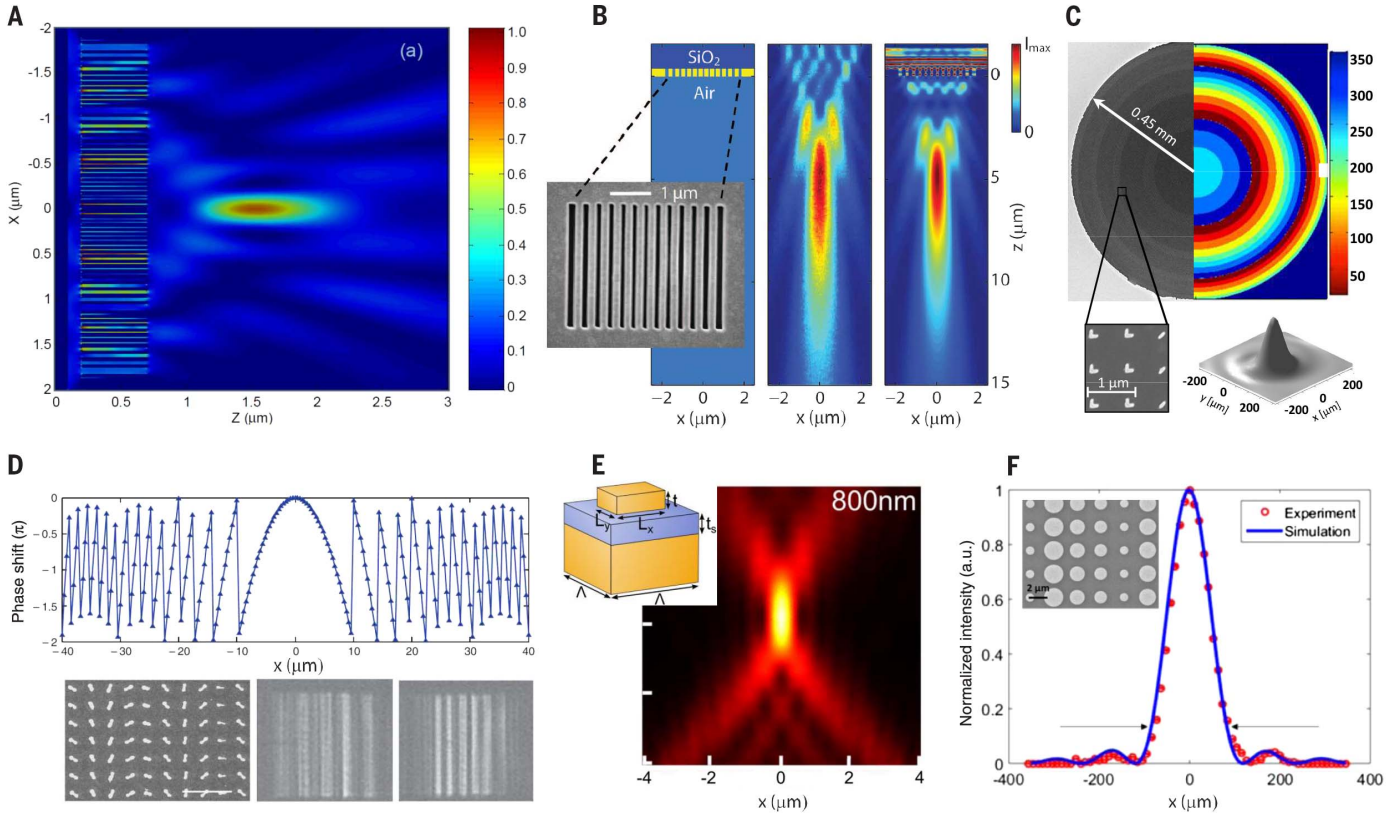

Fig. 1. Plasmonic flat lenses. (**A**) Simulated normalized Poynting vector distribution at λ = 650 nm for a metalens consisting of an array of 65 silver slits with a fixed depth of 500 nm and widths ranging from 10 to 70 nm. The lens functions as a cylindrical lens, focusing the incident light into a line. [Reproduced from (*29*)] (**B**) Schematic of a cylindrical metalens made of gold slits (left) with a depth of 400 nm and widths varying from 80 to 150 nm. The inset shows a scanning electron microscopy (SEM) image of the fabricated metalens. Measured (center) and simulated (right) intensity distributions of focusing patterns at the design wavelength of 637 nm are shown. I_{max}, maximum intensity. [Adapted from (*30*)] (**C**) Phase profile of a near-infrared (NIR) (λ = 1550 nm) metalens with eight V-antennas (*33*). Shown at the bottom are the measured diffraction-limited irradiance in the focal region (right) and an SEM image of a portion of the metalens (left). The antennas' thickness is deep subwavelength $(\frac{\lambda}{25})$. (**D**) (Bottom) SEM image (left) of a portion of a metalens and images formed by the cylindrical lens (λ = 810 nm) under left (center) and right (right) circularly polarized light. Magnification of the imaging system is controlled by the helicity of illuminating light. (Top) Expected realized phase profile of one the metalenses for right circularly polarized incident light. [Adapted from (*39*)] (**E**) Measured intensity distribution near the focus of a cylindrical metalens designed at a wavelength of 800 nm. The inset shows the unit cell: a gold antenna on a gold mirror with a dielectric spacer. Λ, unit cell period; L, lateral dimension of gold antenna; t, height of gold antenna; t_s, thickness of dielectric spacer. [Adapted from (*43*)] (**F**) Measured intensity distribution across the focal line of a reflective metalens designed for λ = 4.6 μm (*44*). Focusing efficiency as high as 80% was achieved close to theoretical prediction of 83%. The inset shows an SEM image of a portion of the lens. a.u., arbitrary units.

This phase can be controlled by adjusting the fill factor (FF). To achieve a phase difference $\Delta\varphi = 2\pi$ between unit cells with FF of unity and zero, the height must then be

$$H = \frac{\lambda}{\Delta n_{\text{eff}}} \qquad (3)$$

where $\Delta n_{\text{eff}} = n - 1$. Assuming a dielectric with a refractive index larger than 2 ($n > 2$, $\Delta n_{\text{eff}} > 1$), the required height becomes comparable to the wavelength. On the basis of this design rule, highly efficient blazed gratings and diffractive lenses have been reported (*19*–*22*).

Plasmonic flat lenses

One of the most commonly used MBBs is the plasmonic antenna (*23*). Like their radio-wave counterparts, these optical antennas concentrate propagating light into regions much smaller than the wavelength, where charge oscillations known as surface plasmons are set up. By designing the antenna's size, shape, and orientation, one can alter the phase shift of the radiated light, thus introducing an abrupt phase change over a distance much smaller than the wavelength. Because of their deep-subwavelength thickness [low aspect ratio (AR)], fabrication of plasmonic antennas is very straightforward: a simple liftoff process is adequate.

Stimulated by the discovery of extraordinary optical transmission through subwavelength metallic apertures (*24*), plasmonics has been the subject of extensive experimental and theoretical research. Plasmonic metalenses have attracted considerable attention as proof-of-principle demonstrations of the advantages of flat lens technology. For example, Yin *et al.* (*25*) showed that surface plasmon polaritons excited by an array of holes constructively interfere to generate an in-plane focal spot (near-field focusing). Liu *et al.* (*26*) also reported in-plane focusing using circular and elliptical slit apertures. In addition, far-field focusing of visible light using quasi-periodic arrays of nanoholes was reported in (*27*). In these previous works (*25*–*27*), focusing is achieved via amplitude modulation and suitable spatial distribution of apertures. A metalens is a phase plate designed to focus light. Attaining a diffraction-limited focus with low wavefront error requires 2π phase coverage with ideally the same scattering amplitude for all phase shifters. For a high-efficiency transmissive metalens, this means having MBBs with negligible optical absorption loss and maximum forward scattering. Sun *et al.* theoretically demonstrated that focusing via phase modulation can be achieved by varying the depth (propagation length) of plasmonic slits (*28*). They further suggested an alternative approach for spatial phase modulation by adjusting

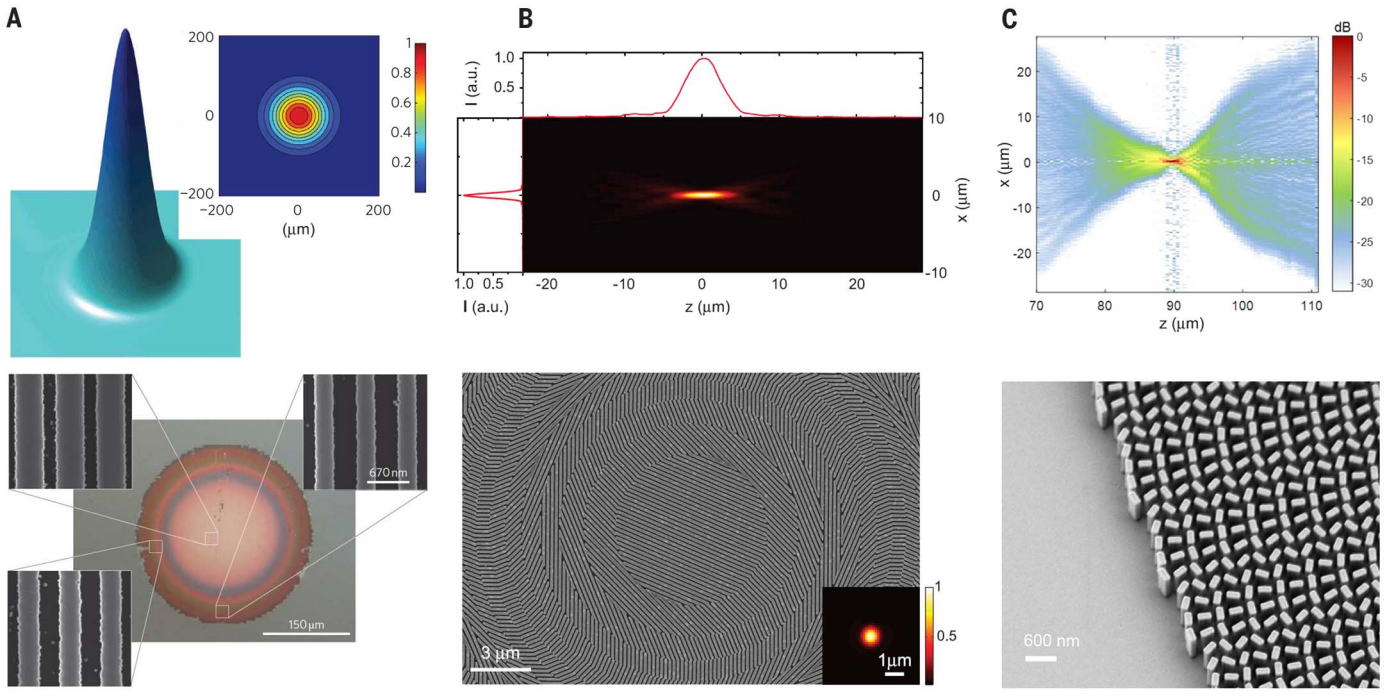

Fig. 2. Dielectric polarization-dependent flat lens. (**A**) (Bottom) Optical microscope image of a reflective lens consisting of an array of amorphous silicon (aSi) groves with spatially varying width. The insets show SEM images of various locations of the lens. The lens is designed in the NIR region and has a numerical aperture (NA) of ~0.01. (Top) Measured beam profile in the focal plane of a reflective lens. The inset shows the measured beam radius ($1/e^2$) along the propagation direction. [Adapted from (*57*)] (**B**) (Bottom) SEM image of the center portion of the fabricated lens. The inset shows the measured focal spot intensity profile. (Top) Measured intensity distribution along the propagation direction, showing the evolution of the beam before and after the focal spot. [Reproduced from (*51*)] (**C**) (Bottom) SEM image of the fabricated lens. This monochromatic metalens operates based on the Pancharatnam-Berry phase, using titanium dioxide nanofins, and can be designed across the visible spectrum with high efficiency. For instance, three lenses with *NA* = 0.8 and diffraction-limited focusing at wavelengths of 405, 532, and 660 nm were reported with corresponding efficiencies of 86, 73, and 66%, respectively. (Top) Measured intensity distribution in decibels along the propagation direction (*52*).

the slits' width, which substantially simplifies the fabrication process. This idea was later theoretically confirmed by Shi *et al.* (*29*) in their simulation of a flat lens consisting of an array of slits with locally varying width (Fig. 1A). The narrower the slit, the larger the phase shift (*29*): For example, slits with 20- and 40-nm widths yield phase shifts of 0.87π and 0.49π, respectively, over a propagation length (slit depth) of 300 nm. This slit geometry translates to an AR of 15, which is difficult to fabricate. Shi *et al.* also showed that by increasing the AR to 50 (minimum width = 10 nm and depth = 500 nm), one can approach the full-phase coverage. Later, Verslegers *et al.* (*30*) experimentally demonstrated a lens based on a phase modulation concept through array of slits with varying width (Fig. 1B). Slits have a depth of 400 nm and a minimum width of 80 nm. Although this low AR (5) simplifies fabrication, it limits the maximum phase shift to ~0.2π.

In the case of a single resonance antenna with a subwavelength thickness, the phase coverage of transmitted light is typically limited to π. Expansion of the phase coverage to 2π is one of the essential steps toward realizing full control of the wavefront. In their work on gradient metasurfaces that diffract light according to the generalized laws of reflection and refraction, Yu and co-workers (*31*, *32*) showed that an array of V-antennas with suitable geometry and orientations provides not only 2π phase coverage but also a large range of scattering amplitudes, both of which are key factors for full control over the wavefront. The thickness of these antennas is much less than the wavelength, which considerably simplifies the fabrication. Using V-antennas, flat lenses free of spherical aberration (Fig. 1C) and axicons were demonstrated in the NIR range (*33*). The focusing efficiency was low as a result of small scattering efficiency of single-layer antennas; this can be improved by increasing the number of layers (*34*). It was also shown that V-apertures, complementary of V-antennas, can be used to focus visible light (*35*) on the basis of Babinet's principle. Alternatively, 2π phase coverage may be achieved by using the Pancharatnam-Berry (PB) phase (*36*, *37*), also known as geometric phase. In this approach, all MBBs have identical sizes (and, therefore, uniform transmitted amplitude), and the phase variation is achieved via their rotation. Flat lenses based on the PB phase were theoretically and experimentally (Fig. 1D) reported using U-apertures (*38*) and rod antennas (*39*), respectively. Simulations in (*38*) show that a lens consisting of an array of identical U-apertures with different orientations focuses left circularly polarized light into a line, whereas the lens diverges right circularly polarized light, an intrinsic property of a PB-based lens (*40*). A PB-based metasurface generates a wavefront with polarization orthogonal to the incident light. Sun *et al.* (*41*, *42*) demonstrated 2π phase coverage using reflect arrays of antennas separated from a metallic mirror by a dielectric spacer, an approach that preserves the incident polarization. This method was later used in flat reflective lenses (Fig. 1E) in the NIR (*43*) and in the mid-infrared region (*44*). In the latter work, the authors demonstrated high efficiency and near diffraction-limited focusing (Fig. 1F). Their use of single-step photolithography allows fabrication of large diameter lenses for applications such as Cassegrain telescopes. Despite major progress in plasmonic metasurfaces, fundamental limits of efficiency (*45*) at visible and NIR wavelengths for transmission operation pose a key obstacle for their practical applications. These problems can be solved by using dielectric metasurfaces (*46*, *47*).

All-dielectric metalenses

Use of dielectric phase shifters (*46*) as MBBs represents a key shift in the metaoptics design approach, which can lead to numerous technological advances. These dielectric MBBs can

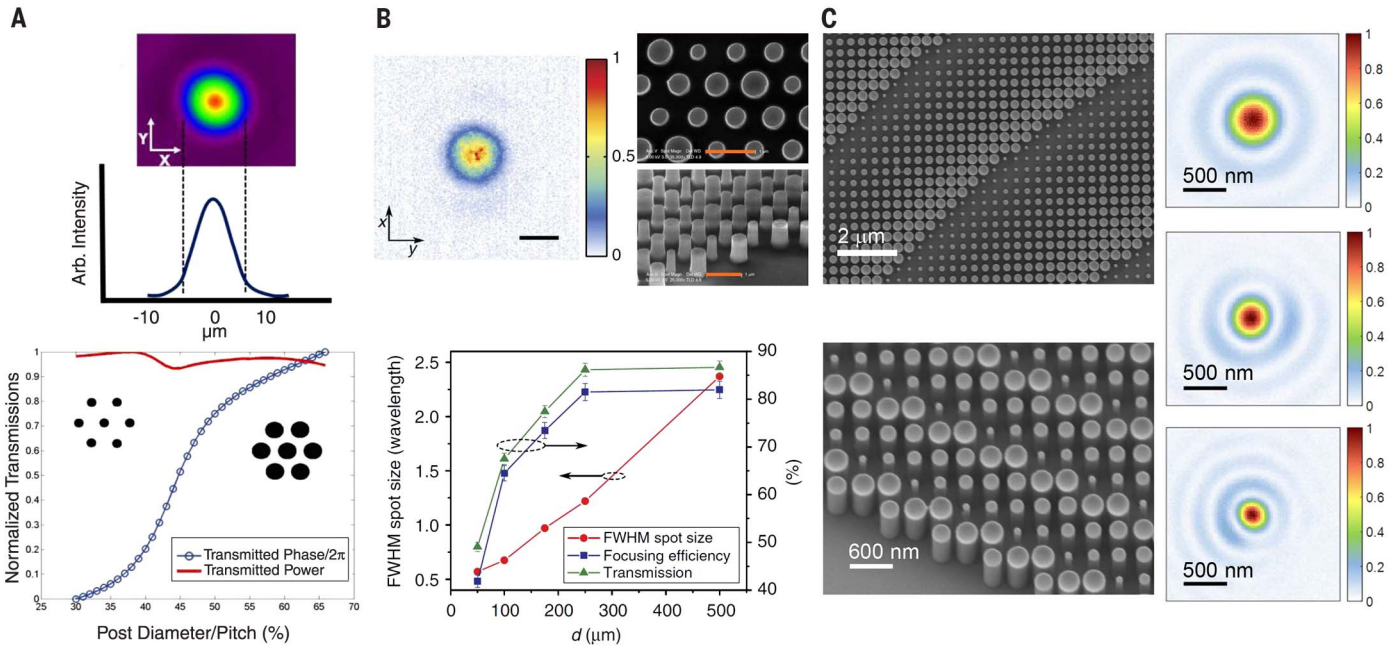

Fig. 3. All-dielectric polarization-independent transmissive metalens. (**A**) (Top) Measured intensity profile of a focal spot with its corresponding horizontal cut. The lens consists of an array of silicon posts with spatially varying diameter fabricated on a glass substrate. (Bottom) Simulated transmitted phase and power for a hexagonal array of silicon posts with different diameters. Posts have a height and pitch of 475 and 390 nm, respectively. [Adapted from (*66*)] (**B**) (Top left) Measured intensity profile at the focal plane of a lens with *NA* ~ 0.97. Scale bar, 1 μm. (Top right) SEM images of the fabricated lens. Silicon posts are arranged in a hexagonal lattice. Scale bars, 1 μm. (Bottom) Measurement results show that there is a trade-off between achieving a higher NA (smaller focal spot) and efficiency, which is a general feature of flat lenses regardless of their design and material platform. FWHM, full width at half maximum; *d*, distance. [Adapted from (*58*)] (**C**) (Left) SEM images show top-in view (top) and side view (bottom) of the fabricated lens. (Right) Measured focal spot profiles of three lenses (*NA* = 0.85) at their design wavelengths of 660 nm (top), 532 nm (center), and 405 nm (bottom). [Adapted from (*63*)]

confine light in a subwavelength region with negligible absorption loss. Here, we primarily focus on the regime where the phase shifters can be treated as truncated waveguides: scatterers with low–quality factor resonances. In other words, the phase accumulation is achieved via propagation, as seen from Eq. 2, but Fabry-Perot effects are inevitable because of reflections at the dielectric waveguide (DW) ends, which are caused by refractive index mismatch. Often, a portion of the incident light, typically a Gaussian beam, is not coupled into the waveguide modes and either propagates through the surrounding medium or in the DW as radiation modes. Therefore, the phase imparted into reflected or transmitted light arises from the superposition of all radiation and waveguide modes. Capturing all of these effects is essential for metasurface design and requires rigorous methods such as finite-difference time-domain simulations.

By adjusting the effective index of DWs by varying their geometrical parameters, the phase coverage can span the required 0-to-2π range. If the effective index modulation is larger than unity ($\Delta n_{\mathrm{eff}} > 1$), full phase coverage can be accomplished via a propagation length (height of DWs) comparable to the wavelength (Eq. 3). This phase implementation can also be polarization dependent (*48*) for a DW with an asymmetric cross section, an effect known as form birefringence. Therefore, through appropriate choice of material and geometrical parameters, a DW can act as a half-waveplate required for efficient PB-based metasurfaces (*49*–*54*). This approach was used by Hasman *et al.* (*49*); in their study, birefringent subwavelength gratings served as BBs of a flat lens in the mid-infrared range. Considering the lens design parameters (*NA* = 0.02 and λ = 10.6 μm), the spatial discretization of the phase profile [center to center distance (*U* = ~50 μm)] between adjacent MBBs satisfies the required sampling criterion

$$U < \frac{\lambda}{2NA} \tag{4}$$

This was further confirmed by the observation of a diffraction-limited focal spot. Satisfying this criterion becomes more challenging for lenses designed at shorter wavelengths or with higher NAs. The smaller the value of *U*, the narrower the DWs and, thus, the higher the required AR must be to achieve full phase coverage, which introduces stringent fabrication demands. This limitation also brings new design challenges: As the adjacent DWs become closer together, their lateral size decreases, which leads to less optical confinement and greater near-field coupling between the DWs. Note that satisfying the sampling criterion (Eq. 4) does not eliminate the possibility of higher orders (for *NA* < 0.5, *U* can be larger than the wavelength λ) but only guarantees that one can provide the required phase gradient at each location on the metasurface. In other words, to design a flat lens that focuses a normally incident collimated beam, one needs to generate a spatially varying phase gradient, which represents an effective wave vector (*32*) locally imparted by the metasurface so that at each position, the incident beam is deflected toward the focal point. The maximum deflection angle θ [$\sin(\theta) = NA$] occurs at the edge of the lens. Therefore, the maximum required effective wave vector is $\frac{2\pi}{\lambda}\sin(\theta)$. From the generalized Snell's law (*31*)

$$k\sin(\theta) = \frac{\Delta\varphi}{\Delta x} \tag{5}$$

($k = 2\pi/\lambda$). Considering the finite size of the MBBs, the phase is always discretized and implementable with a digital phase mask (*55*). To deflect normally incident light *s*, one needs to introduce a phase difference between adjacent MBBs. The phase difference Δφ can be as large as π ($\Delta\varphi \le \pi$). Therefore, on the basis of Eq. 5, the distance between adjacent MBBs ($\Delta x = U$) should be equal to or smaller than $\frac{\lambda}{2NA}$ $\left(\Delta x \le \frac{\lambda}{2NA}\right)$ to provide the required effective wave vector and thus deflect light by an angle θ.

In addition, the smaller the value of *U*, the better the sampling and the lower the required phase difference between two adjacent MBBs, resulting

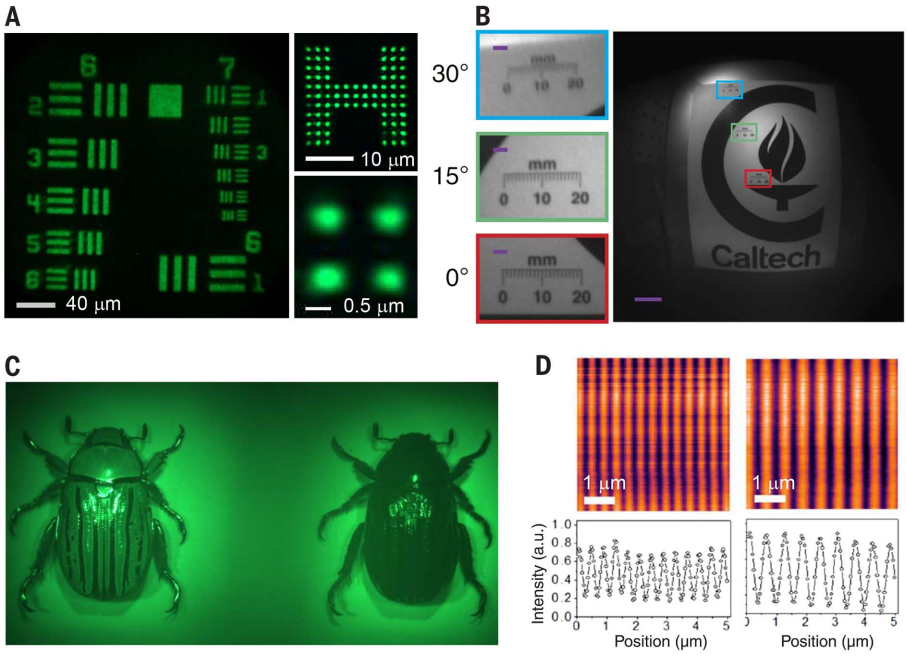

Fig. 4. Imaging with monochromatic all-dielectric metalenses. (**A**) Images formed by a metalens of the 1951 U.S. Air Force resolution test chart (left) and of a customized target object (right) with a minimum gap size of ~800 nm (right top) and ~450 nm (right bottom) (*52*). Illumination was provided by a tunable laser with a 530-nm center wavelength and a bandwidth of 5 nm. (**B**) (Right) Image taken with a doublet lens made of silicon posts operating at a wavelength of 850 nm. Scale bar, 100 μm. (Left) Zoomed-in views of the images at the regions indicated by the rectangles. Scale bars, 10 μm. The illumination source was an LED paired with a 10-nm bandpass filter centered at 850 nm. [Reproduced from (*67*)] (**C**) Two images of a beetle, *Chrysina gloriosa*, formed by a chiral lens in the same field of view of a camera (*73*). This chiral lens simultaneously forms two spatially separated images (with opposite handedness) of the beetle, revealing its natural circular dichroism. The chiral lens has diameter D = 3 mm and a focal length of ~3 cm at its 530-nm design wavelength. Green LEDs paired with a 10-nm bandpass filter centered at 532 nm were used as illumination sources. (**D**) (Top) Images of metallic stripes formed by confocal imaging with an oil immersion lens used for illumination (*69*). (Bottom) Mean peak-to-peak values of 400 nm (left) and 593 nm (right) with less than 10% SD. This metalens is made of titanium dioxide nanofins and has NA = 1.1 at its 532-nm design wavelength.

in a quasi-adiabatic change in geometrical size of MBBs across the interface. Plasmonic MBBs can easily fulfill this criterion because they can be closely packed, owing to the deep-subwavelength confinement of plasmonic modes. High-index dielectrics can also satisfy these conditions by enhancing light confinement and reducing near-field coupling, thus allowing a smaller U.

Due to their large refractive index and mature fabrication technology, silicon-based metasurfaces are a promising platform for realizing metalenses, particularly in the NIR region (*51*, *56*–*60*), the transparency window of silicon. Reflective dielectric planar lenses were theoretically (*56*) and experimentally (*57*) reported using one-dimensional amorphous silicon (aSi) gratings for which the period and the FF of the grating elements were gradually altered from the center of the lens toward the edge (Fig. 2A). Because of the asymmetric cross section of the grating elements, the performance of these lenses depends on polarization. A transmissive lens was also demonstrated in aSi using the PB phase (Fig. 2B). The lens is designed at λ = 550 nm and has NA = 0.43 (*51*). In the visible region, especially at shorter wavelengths, the optical loss of silicon substantially degrades the lenses' efficiency. This can be partially overcome by changing the material to a dielectric with transparency in the visible region; examples include silicon nitride (*61*) and titanium dioxide (*21*). However, the refractive index of these materials (n ~ 2) is lower than that of silicon (n ~ 3.5). In general, to achieve full 0-to-2π phase coverage using these materials, one needs to compensate for the smaller index with higher DW height (Eq. 2). As a result, high-AR structures are required, which poses major challenges for conventional fabrication techniques such as dry-etching (*21*, *61*) and liftoff (*62*). The latter substantially limits the maximum attainable height of DWs, and the former does not provide adequate control over the geometry of DWs. One prevailing problem is the angled sidewall, which introduces an error in the resultant phase (*63*). A recently developed process based on atomic layer deposition (ALD) of titanium dioxide (*64*) has successfully circumvented these issues. DWs are defined only by the patterned resist in this liftoff-like process, which can then be extended to a wide range of dielectrics supported by the ALD technique. With the use of this approach, large NA = 0.8 lenses with efficiency as high 86% were demonstrated (*52*, *65*) across the visible spectrum (Fig. 2C).

To realize polarization-independent lenses, one can utilize the propagation phase using DWs with circular or fourfold-symmetric cross sections. By using arrays of circular silicon posts, Vo *et al.* (*66*) demonstrated polarization-independent transmissive lenses with 70% efficiency. The lens focuses the incident light (λ = 850 nm) into a spot of ~10λ size. The lens's BB was a hexagonal array of posts (Fig. 3A). This BB configuration reduces the maximum achievable spatial phase gradient due to the increased U and thus limits the maximum obtainable NA. Later, Arbabi *et al.* (*58*) showed that one silicon post can serve as an efficient BB (Fig. 3B). This BB provides full phase coverage with subwavelength spatial resolution while maintaining high transmission, thus enabling highly efficient metalenses with large NAs. Lenses with efficiencies higher than 42% and focal spots as small as 0.57λ at λ = 1550 nm were reported. Owing to their high refractive indices, these posts are weakly coupled to each other, which prevents deviation from the designed phase due to near-field coupling. High-performance metalenses in the visible spectrum were demonstrated by Khorasaninejad *et al.* (*63*). These polarization-independent lenses were fabricated by using ALD-prepared titanium dioxide circular posts and have NAs as high as 0.85. At this NA, metalenses designed at wavelengths of 532 and 660 nm provide diffraction-limited focusing with efficiency larger than 60% (Fig. 3C). For the metalenses designed at a shorter wavelength (405 nm), the efficiency drops to 33% due to stringent fabrication tolerances because the posts' radii scale proportionally with wavelength. In addition, when the NA was reduced to 0.6, focusing efficiency as high as 90% was achieved at a design wavelength of 660 nm.

Imaging by metalenses

Theoretically, the imaging resolution of a lens is set by the diffraction limit, but in practice, various aberrations such as spherical and coma reduce it. Spherical aberration is a common issue in refractive lenses (particularly high-NA objectives) and is typically corrected by cascading several lenses, which not only increases the size of imaging systems but also adds cost. Metalenses can be free of spherical aberrations because their phases can be tailored at the designer's will. Figure 4A shows images formed by a high-NA (0.81) flat lens designed at λ = 532 nm. This lens resolves micrometer-size features over a large area of 250 μm × 250 μm. The same lens also resolves the details of an object with subwavelength resolution; however, its field of view (FOV) is very limited. The latter is a manifestation of other remaining monochromatic aberrations, mainly coma. These aberrations can be reduced by adding a correcting layer (*67*, *68*) to a flat lens

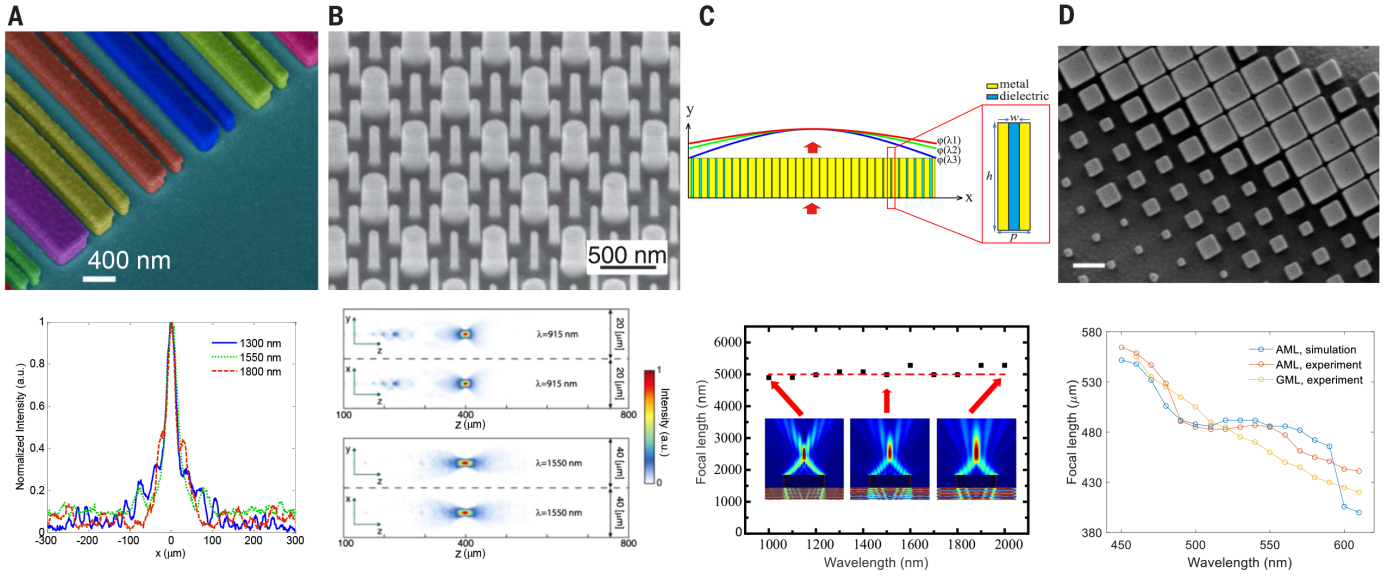

Fig. 5. Dispersion engineering. (**A**) (Top) False-color side-view SEM image of a portion of a multiwavelength achromatic metalens (AML) (*81*). Each unit cell (an aSi rectangular dielectric resonator) is depicted in a different color. (Bottom) Measured intensity profiles at a fixed distance from the metalens for three wavelengths: 1300, 1550, and 1800 nm. The measured full widths at half maximum are 27.5, 29, and 25 μm at λ = 1300, 1550, and 1800 nm, respectively, which are close to the diffraction limit (17, 20, and 23 μm). (**B**) (Top) Tilted-view SEM image of part of a multiwavelength AML showing aSi posts. This lens has a *NA* = 0.46 and focuses two wavelengths of 1550 and 915 nm at the same focal distance. (Bottom) Intensity measured in the axial planes of the lens for wavelengths of 915 and 1550 nm. [Adapted from (*91*)] (**C**) (Top) Side-view schematic of a broadband achromatic metalens. The inset shows the unit cell: a metal-insulator-metal waveguide. φ, phase shift; *w*, *h*, and *p* represent the width of dielectric, length of the waveguide, and period of the unit cell, respectively. (Bottom) Simulated focal lengths of the lens versus wavelength. The insets show the calculated electric field intensity distributions at wavelengths λ = 1, 1.5, and 2 μm. [Adapted from (*89*)] (**D**) (Top) Top-view SEM image of an AML operating over a continuous band (60 nm) in the visible spectrum (*88*). The building block of the lens is a titanium dioxide pillar on a metallic mirror with an intermediate silicon dioxide thin film. Scale bar, 500 nm. (Bottom) Simulated and measured focal length of the AML as a function of wavelength. The measured fractional changes of focal length across the bandwidth (490 to 550 nm) are 1.5 and 1.2%, respectively. The measured focal length of a lens [geometric-phase lens (GML)] with no chromatic correction is also shown for comparison.

(doublet metalens) or avoided by scanning microscopy imaging (*69*). In (*67*), the doublet flat lenses consist of two metasurface layers fabricated on opposite sides of a glass substrate (Fig. 4B). These lenses provide nearly diffraction-limited imaging at the design NIR wavelength over an FOV of 60°. Recently, a similar design with a 50° FOV was demonstrated in the green portion of the visible region (*68*). In (*69*), Chen *et al.* integrated an immersion flat lens with a commercial confocal microscope and achieved imaging resolution down to 200 nm over a large area (Fig. 4D). A similar design principle can be used to achieve diffraction-limited focusing in any medium, including multiple layers of complex media consisting of liquid and solids (e.g., biological tissue). In conventional state-of-the art immersion objectives, the front lens often needs to be polished by hand (*70*) to meet specifications.

Multifunctional metalenses and control of chromatic dispersion

Generally, multifunctional imaging systems are realized by cascading optical components. One useful function of these systems is resolving polarization information (*71*) of a scene, which can improve image quality in optically scattering conditions such as hazy and foggy environments and turbid media. Typical polarization imaging systems consist of multiple optical components, including polarizers and waveplates, leading to complex setups and limiting their integration into miniaturized systems. Schonbrun *et al.* used elliptical silicon nanowires to encode a polarization-dependent phase (*72*). Using this method, a flat lens with focal length varying with incident polarization was achieved. Resolving chirality of light becomes even more challenging due to the required extra phase information. Using the PB phase concept, Khorasaninejad *et al.* demonstrated a metalens that can simultaneously form spectrally resolved images with opposite chirality of a biological specimen in the same FOV of a camera (Fig. 4C) (*73*). This result indicates that chiroptical properties such as circular dichroism can be probed across the visible spectrum using only a single lens and a camera, without the addition of polarizers or dispersive optical components.

One can utilize the chromatic dispersion of metalenses to resolve the wavelength with high precision. In (*74*), Khorasaninejad *et al.* showed that metalens chromaticity can be considerably enhanced by operating in off-axis mode. These off-axis lenses simultaneously focus and disperse light of different wavelengths with unprecedented spectral resolution down to 0.2 nm in the NIR region (*74*). Later, this design was extended into the visible wavelength by titanium dioxide–based off-axis lenses (*75*). A compact spectrometer was achieved in which the required beam propagation distance is on the order of a few centimeters, with spectral resolutions as small as 0.3 nm. Additionally, this metaspectrometer can simultaneously resolve the chirality of light. The latter was achieved via spatial multiplexing; more efficient performance can be achieved by combination of PB and propagation phase, as discussed in (*76*, *77*).

Although the strong intrinsic dispersive response of a metasurface is beneficial for some applications, it is a fundamental limiting factor for others, such as imaging and microscopy. Therefore, correcting chromatic aberration or, in general, controlling the chromatic dispersion is of great interest (*78*–*90*). Toward this goal, a dispersive phase-compensation approach by means of coupled dielectric resonators was implemented to correct the chromatic aberration at several discrete wavelengths (*80*). A multiwavelength achromatic metalens, functioning as a cylindrical lens (Fig. 5A) in the NIR region, was demonstrated via this approach (*81*). This concept was later extended by Arbabi *et al.* (*91*) to demonstrate a spherical lens (Fig. 5B). Other alternative approaches based on spatial multiplexing (*83*–*86*) and stacking (*92*) were proposed; however, multiplexing-based designs generally limit efficiency. Achieving achromatic focusing over a large bandwidth has proven challenging. A broadband achromatic metalens was theoretically

proposed using a metal-insulator-metal waveguide (Fig. 5C) through compensation of material and structural dispersion (*89*). In addition, a broadband achromatic metalens functioning as a cylindrical lens in the visible region with *NA* = 0.013 was achieved using graded dielectric interfaces made of resist with spatially varying height fabricated by grayscale lithography (*93*). Recently, through the use of guided-mode resonances (*94*) supported by titanium dioxide DWs spanning many 2π phase shifts, a new approach for dispersion engineering (*88*) was proposed, and an achromatic reflective metalens with *NA* = 0.2 was experimentally reported with a bandwidth of 60 nm in the visible region, close to the spectrum of a green light-emitting diode (LED) (Fig. 5D). In addition, a lens with reverse chromatic dispersion was proposed on the basis of this dispersion engineering approach (*88*), providing yet another illustration that one can break away from the constraints of conventional diffractive optics.

Conclusions and outlook

Flat lenses based on all-dielectric metasurfaces have proven their potential to replace and complement their traditional counterparts. Some important features of this platform are its straightforward complementary metal-oxide semiconductor–compatible fabrication method, attendant reduction in thickness, and easier optical alignment and packaging in camera modules. Despite substantial progress in metalens performance, many areas remain to be explored and improved. This is especially true for dispersion engineering, in which demonstration of achromatic transmissive lenses with relatively large NAs and very high efficiency (>90%) across the visible spectrum would be a game-changer for the camera industry. Future high-volume applications include cell phone camera modules, wearable displays for augmented and virtual reality, machine vision, and automotive and security cameras.

Multilayered metasurface geometries exhibiting angular phase control, such as single-piece nanophotonic metalenses that focus light into the same focal spot regardless of the angle of incidence (*95*), are the subject of much current interest. Other presently relevant topics include metalenses with voltage-controlled focal length, magnification, and aberrations.

Owing to their small footprint and planar geometry, metalenses can be mounted on the facet of an optical fiber, opening up numerous applications such as bioimaging and endoscopy (*96*, *97*). Soft-lithography techniques are well suited for metalens fabrications on optical fiber facets. In designing such metalenses, one can easily account for the complex imaging environment (specific tissue or biological specimen composed of multiplex layers with different thickness and refractive index).

These are only a few examples of areas in which this flat lens technology can have a substantial impact. Our discussion here focused on lenses, but this metasurface platform can be vertically integrated to build a complex system composed of various planar components (e.g., lenses, gratings, polarizers, and filters) to perform sophisticated tasks with ease of fabrication. This capability can fuel the continuous progress of wearable and portable consumer electronics and optics in which low-cost and high-performance miniaturized systems are in high demand.

REFERENCES AND NOTES

1. A. V. Kildishev, A. Boltasseva, V. M. Shalaev, Planar photonics with metasurfaces. *Science* **339**, 1232009 (2013). doi: 10.1126/science.1232009; pmid: 23493714
2. N. Yu, F. Capasso, Flat optics with designer metasurfaces. *Nat. Mater.* **13**, 139–150 (2014). doi: 10.1038/nmat3839; pmid: 24452357
3. P. Genevet, F. Capasso, F. Aieta, M. Khorasaninejad, R. Devlin, Recent advances in planar optics: From plasmonic to dielectric metasurfaces. *Optica* **4**, 139–152 (2017). doi: 10.1364/OPTICA.4.000139
4. F. Falcone *et al*., Babinet principle applied to the design of metasurfaces and metamaterials. *Phys. Rev. Lett.* **93**, 197401 (2004). doi: 10.1103/PhysRevLett.93.197401; pmid: 15600876
5. H. H. Hsiao, C. H. Chu, D. P. Tsai, Fundamentals and applications of metasurfaces. *Small Methods* **1**, 1600064 (2017). doi: 10.1002/smtd.201600064
6. D. Berry, R. Malech, W. Kennedy, The reflectarray antenna. *IEEE Trans. Antenn. Propag.* **11**, 645–651 (1963). doi: 10.1109/TAP.1963.1138112
7. D. Pozar, T. Metzler, Analysis of a reflectarray antenna using microstrip patches of variable size. *Electron. Lett.* **29**, 657–658 (1993). doi: 10.1049/el:19930440
8. C. Pfeiffer, A. Grbic, Metamaterial Huygens' surfaces: Tailoring wave fronts with reflectionless sheets. *Phys. Rev. Lett.* **110**, 197401 (2013). doi: 10.1103/PhysRevLett.110.197401; pmid: 23705738
9. M. Decker *et al*., High-efficiency dielectric Huygens' surfaces. *Adv. Opt. Mater.* **3**, 813–820 (2015). doi: 10.1002/adom.201400584
10. Y. H. Fu, A. I. Kuznetsov, A. E. Miroshnichenko, Y. F. Yu, B. Luk'yanchuk, Directional visible light scattering by silicon nanoparticles. *Nat. Commun.* **4**, 1527 (2013). doi: 10.1038/ncomms2538; pmid: 23443555
11. S. Person *et al*., Demonstration of zero optical backscattering from single nanoparticles. *Nano Lett.* **13**, 1806–1809 (2013). doi: 10.1021/nl4005018; pmid: 23461654
12. W. E. Kock, Metallic delay lenses. *Bell Syst. Tech. J.* **27**, 58–82 (1948). doi: 10.1002/j.1538-7305.1948.tb01331.x
13. K. Miyamoto, The phase Fresnel lens. *J. Opt. Soc. Am.* **51**, 17–20 (1961). doi: 10.1364/JOSA.51.000017
14. L. d'Auria, J. Huignard, A. Roy, E. Spitz, Photolithographic fabrication of thin film lenses. *Opt. Commun.* **5**, 232–235 (1972). doi: 10.1016/0030-4018(72)90086-7
15. E. Wolf, M. Born, *Principles of Optics* (Pergamon Press, ed. 6, 1993).
16. G. J. Swanson, "Binary optics technology: Theoretical limits on the diffraction efficiency of multilevel diffractive optical elements" (Tech. Rep. 914, Defense Technical Information Center, 1991).
17. W. Stork, N. Streibl, H. Haidner, P. Kipfer, Artificial distributed-index media fabricated by zero-order gratings. *Opt. Lett.* **16**, 1921–1923 (1991). doi: 10.1364/OL.16.001921; pmid: 19784181
18. M. W. Farn, Binary gratings with increased efficiency. *Appl. Opt.* **31**, 4453–4458 (1992). doi: 10.1364/AO.31.004453; pmid: 20725441
19. F. T. Chen, H. G. Craighead, Diffractive phase elements based on two-dimensional artificial dielectrics. *Opt. Lett.* **20**, 121–123 (1995). doi: 10.1364/OL.20.000121; pmid: 19859107
20. F. T. Chen, H. G. Craighead, Diffractive lens fabricated with mostly zeroth-order gratings. *Opt. Lett.* **21**, 177–179 (1996). doi: 10.1364/OL.21.000177; pmid: 19865344
21. P. Lalanne, S. Astilean, P. Chavel, E. Cambril, H. Launois, Blazed binary subwavelength gratings with efficiencies larger than those of conventional échelette gratings. *Opt. Lett.* **23**, 1081–1083 (1998). doi: 10.1364/OL.23.001081; pmid: 18087434
22. P. Lalanne, S. Astilean, P. Chavel, E. Cambril, H. Launois, Design and fabrication of blazed binary diffractive elements with sampling periods smaller than the structural cutoff. *J. Opt. Soc. Am. A* **16**, 1143–1156 (1999). doi: 10.1364/JOSAA.16.001143
23. L. Novotny, N. Van Hulst, Antennas for light. *Nat. Photonics* **5**, 83–90 (2011). doi: 10.1038/nphoton.2010.237
24. T. W. Ebbesen, H. J. Lezec, H. Ghaemi, T. Thio, P. Wolff, Extraordinary optical transmission through sub-wavelength hole arrays. *Nature* **391**, 667–669 (1998). doi: 10.1038/35570
25. L. Yin *et al*., Subwavelength focusing and guiding of surface plasmons. *Nano Lett.* **5**, 1399–1402 (2005). doi: 10.1021/nl050723m; pmid: 16178246
26. Z. Liu *et al*., Focusing surface plasmons with a plasmonic lens. *Nano Lett.* **5**, 1726–1729 (2005). doi: 10.1021/nl051013j; pmid: 16159213
27. F. M. Huang, N. Zheludev, Y. Chen, F. Javier Garcia de Abajo, Focusing of light by a nanohole array. *Appl. Phys. Lett.* **90**, 091119 (2007). doi: 10.1063/1.2710775
28. Z. Sun, H. K. Kim, Refractive transmission of light and beam shapingwith metallic nano-optic lenses. *Appl. Phys. Lett.* **85**, 642–644 (2004). doi: 10.1063/1.1776327
29. H. Shi *et al*., Beam manipulating by metallic nano-slits with variant widths. *Opt. Express* **13**, 6815–6820 (2005). doi: 10.1364/OPEX.13.006815; pmid: 19498698
30. L. Verslegers *et al*., Planar lenses based on nanoscale slit arrays in a metallic film. *Nano Lett.* **9**, 235–238 (2009). doi: 10.1021/nl802830y; pmid: 19053795
31. N. Yu *et al*., Light propagation with phase discontinuities: Generalized laws of reflection and refraction. *Science* **334**, 333–337 (2011). doi: 10.1126/science.1210713; pmid: 21885733
32. F. Aieta *et al*., Out-of-plane reflection and refraction of light by anisotropic optical antenna metasurfaces with phase discontinuities. *Nano Lett.* **12**, 1702–1706 (2012). doi: 10.1021/nl300204s; pmid: 22335616
33. F. Aieta *et al*., Aberration-free ultrathin flat lenses and axicons at telecom wavelengths based on plasmonic metasurfaces. *Nano Lett.* **12**, 4932–4936 (2012). doi: 10.1021/nl302516v; pmid: 22894542
34. B. Memarzadeh, H. Mosallaei, Array of planar plasmonic scatterers functioning as light concentrator. *Opt. Lett.* **36**, 2569–2571 (2011). doi: 10.1364/OL.36.002569; pmid: 21725482
35. X. Ni, S. Ishii, A. V. Kildishev, V. M. Shalaev, Ultra-thin, planar, Babinet-inverted plasmonic metalenses. *Light Sci. Appl.* **2**, e72 (2013). doi: 10.1038/lsa.2013.28
36. S. Pancharatnam, in *Proceedings of the Indian Academy of Sciences - Section A* (Springer, 1956), vol. 44, pp. 398–417.
37. M. V. Berry, The adiabatic phase and Pancharatnam's phase for polarized light. *J. Mod. Opt.* **34**, 1401–1407 (1987). doi: 10.1080/09500348714551321
38. M. Kang, T. Feng, H.-T. Wang, J. Li, Wave front engineering from an array of thin aperture antennas. *Opt. Express* **20**, 15882–15890 (2012). doi: 10.1364/OE.20.015882; pmid: 22772278
39. X. Chen *et al*., Dual-polarity plasmonic metalens for visible light. *Nat. Commun.* **3**, 1198 (2012). doi: 10.1038/ncomms2207; pmid: 23149743
40. F. Gori, Measuring Stokes parameters by means of a polarization grating. *Opt. Lett.* **24**, 584–586 (1999). doi: 10.1364/OL.24.000584; pmid: 18073790
41. S. Sun *et al*., High-efficiency broadband anomalous reflection by gradient meta-surfaces. *Nano Lett.* **12**, 6223–6229 (2012). doi: 10.1021/nl3032668; pmid: 23189928
42. S. Sun *et al*., Gradient-index meta-surfaces as a bridge linking propagating waves and surface waves. *Nat. Mater.* **11**, 426–431 (2012). doi: 10.1038/nmat3292; pmid: 22466746
43. A. Pors, M. G. Nielsen, R. L. Eriksen, S. I. Bozhevolnyi, Broadband focusing flat mirrors based on plasmonic gradient metasurfaces. *Nano Lett.* **13**, 829–834 (2013). doi: 10.1021/nl304761m; pmid: 23343380
44. S. Zhang *et al*., High efficiency near diffraction-limited mid-infrared flat lenses based on metasurface reflectarrays. *Opt. Express* **24**, 18024–18034 (2016). doi: 10.1364/OE.24.018024; pmid: 27505769
45. F. Monticone, N. M. Estakhri, A. Alù, Full control of nanoscale optical transmission with a composite metascreen. *Phys. Rev. Lett.* **110**, 203903 (2013). doi: 10.1103/PhysRevLett.110.203903; pmid: 25167411
46. S. Jahani, Z. Jacob, All-dielectric metamaterials. *Nat. Nanotechnol.* **11**, 23–36 (2016). doi: 10.1038/nnano.2015.304; pmid: 26740041
47. A. I. Kuznetsov, A. E. Miroshnichenko, M. L. Brongersma, Y. S. Kivshar, B. Luk'yanchuk, Optically resonant dielectric nanostructures. *Science* **354**, aag2472 (2016). doi: 10.1126/science.aag2472; pmid: 27856851
48. D. C. Flanders, Submicrometer periodicity gratings as artificial anisotropic dielectrics. *Appl. Phys. Lett.* **42**, 492–494 (1983). doi: 10.1063/1.93979

49. E. Hasman, V. Kleiner, G. Biener, A. Niv, Polarization dependent focusing lens by use of quantized Pancharatnam–Berry phase diffractive optics. *Appl. Phys. Lett.* **82**, 328–330 (2003). doi: 10.1063/1.1539300
50. U. Levy, H.-C. Kim, C.-H. Tsai, Y. Fainman, Near-infrared demonstration of computer-generated holograms implemented by using subwavelength gratings with space-variant orientation. *Opt. Lett.* **30**, 2089–2091 (2005). doi: 10.1364/OL.30.002089; pmid: 16127919
51. D. Lin, P. Fan, E. Hasman, M. L. Brongersma, Dielectric gradient metasurface optical elements. *Science* **345**, 298–302 (2014). doi: 10.1126/science.1253213; pmid: 25035488
52. M. Khorasaninejad *et al*., Metalenses at visible wavelengths: Diffraction-limited focusing and subwavelength resolution imaging. *Science* **352**, 1190–1194 (2016). doi: 10.1126/science.aaf6644; pmid: 27257251
53. W. Luo, S. Xiao, Q. He, S. Sun, L. Zhou, Photonic spin Hall effect with nearly 100% efficiency. *Adv. Opt. Mater.* **3**, 1102–1108 (2015). doi: 10.1002/adom.201500068
54. G. Zheng *et al*., Metasurface holograms reaching 80% efficiency. *Nat. Nanotechnol.* **10**, 308–312 (2015). doi: 10.1038/nnano.2015.2; pmid: 25705870
55. B. C. Kress, P. Meyrueis, *Applied Digital Optics: From Micro-optics to Nanophotonics* (Wiley, 2009).
56. F. Lu, F. G. Sedgwick, V. Karagodsky, C. Chase, C. J. Chang-Hasnain, Planar high-numerical-aperture low-loss focusing reflectors and lenses using subwavelength high contrast gratings. *Opt. Express* **18**, 12606–12614 (2010). doi: 10.1364/OE.18.012606; pmid: 20588387
57. D. Fattal, J. Li, Z. Peng, M. Fiorentino, R. G. Beausoleil, Flat dielectric grating reflectors with focusing abilities. *Nat. Photonics* **4**, 466–470 (2010). doi: 10.1038/nphoton.2010.116
58. A. Arbabi, Y. Horie, A. J. Ball, M. Bagheri, A. Faraon, Subwavelength-thick lenses with high numerical apertures and large efficiency based on high-contrast transmitarrays. *Nat. Commun.* **6**, 7069 (2015). doi: 10.1038/ncomms8069; pmid: 25947118
59. P. R. West *et al*., All-dielectric subwavelength metasurface focusing lens. *Opt. Express* **22**, 26212–26221 (2014). doi: 10.1364/OE.22.026212; pmid: 25401653
60. M. Khorasaninejad, K. B. Crozier, Silicon nanofin grating as a miniature chirality-distinguishing beam-splitter. *Nat. Commun.* **5**, 5386 (2014). doi: 10.1038/ncomms6386; pmid: 25388102
61. A. Zhan *et al*., Low-contrast dielectric metasurface optics. *ACS Photonics* **3**, 209–214 (2016). doi: 10.1021/acsphotonics.5b00660
62. N. M. Estakhri, V. Neder, M. W. Knight, A. Polman, A. Alù, Visible light, wide-angle graded metasurface for back reflection. *ACS Photonics* **4**, 228–235 (2017). doi: 10.1021/acsphotonics.6b00965
63. M. Khorasaninejad *et al*., Polarization-insensitive metalenses at visible wavelengths. *Nano Lett.* **16**, 7229–7234 (2016). doi: 10.1021/acs.nanolett.6b03626; pmid: 27791380
64. R. C. Devlin, M. Khorasaninejad, W. T. Chen, J. Oh, F. Capasso, Broadband high-efficiency dielectric metasurfaces for the visible spectrum. *Proc. Natl. Acad. Sci. U.S.A.* **113**, 10473–10478 (2016). doi: 10.1073/pnas.1611740113; pmid: 27601634
65. M. Khorasaninejad *et al*., Visible wavelength planar metalenses based on titanium dioxide. *IEEE J. Sel. Top. Quantum Electron.* **23**, 4700216 (2017). doi: 10.1109/JSTQE.2016.2616447
66. S. Vo *et al*., Sub-wavelength grating lenses with a twist. *IEEE Photonics Technol. Lett.* **26**, 1375–1378 (2014). doi: 10.1109/LPT.2014.2325947
67. A. Arbabi *et al*., Miniature optical planar camera based on a wide-angle metasurface doublet corrected for monochromatic aberrations. *Nat. Commun.* **7**, 13682 (2016). doi: 10.1038/ncomms13682; pmid: 27892454
68. B. Groever, W. T. Chen, F. Capasso, Meta-lens doublet in the visible region. *Nano Lett.* **17**, 4902–4907 (2017). doi: 10.1021/acs.nanolett.7b01888; pmid: 28661676
69. W. T. Chen *et al*., Immersion meta-lenses at visible wavelengths for nanoscale imaging. *Nano Lett.* **17**, 3188–3194 (2017). doi: 10.1021/acs.nanolett.7b00717; pmid: 28388086
70. "Lens polishing – Hand-polishing spherical front lenses for microscopes" (2017); www.nikoninstruments.com/Learn-Explore/Nikon-Craftsmanship/Lens-Polishing-Hand-polishing-spherical-front-lenses-for-microscopes.
71. R. M. Azzam, N. M. Bashara, *Ellipsometry and Polarized Light* (North-Holland, 1987).
72. E. Schonbrun, K. Seo, K. B. Crozier, Reconfigurable imaging systems using elliptical nanowires. *Nano Lett.* **11**, 4299–4303 (2011). doi: 10.1021/nl202324s; pmid: 21923112
73. M. Khorasaninejad *et al*., Multispectral chiral imaging with a metalens. *Nano Lett.* **16**, 4595–4600 (2016). doi: 10.1021/acs.nanolett.6b01897; pmid: 27267137
74. M. Khorasaninejad, W. T. Chen, J. Oh, F. Capasso, Super-dispersive off-axis meta-lenses for compact high resolution spectroscopy. *Nano Lett.* **16**, 3732–3737 (2016). doi: 10.1021/acs.nanolett.6b01097; pmid: 27119987
75. A. Y. Zhu *et al*., Ultra-compact visible chiral spectrometer with meta-lenses. *APL Photonics* **2**, 036103 (2017). doi: 10.1063/1.4974259
76. A. Arbabi, Y. Horie, M. Bagheri, A. Faraon, Dielectric metasurfaces for complete control of phase and polarization with subwavelength spatial resolution and high transmission. *Nat. Nanotechnol.* **10**, 937–943 (2015). doi: 10.1038/nnano.2015.186; pmid: 26322944
77. J. P. Balthasar Mueller, N. A. Rubin, R. C. Devlin, B. Groever, F. Capasso, Metasurface polarization optics: Independent phase control of arbitrary orthogonal states of polarization. *Phys. Rev. Lett.* **118**, 113901 (2017). doi: 10.1103/PhysRevLett.118.113901; pmid: 28368630
78. D. Faklis, G. M. Morris, Spectral properties of multiorder diffractive lenses. *Appl. Opt.* **34**, 2462–2468 (1995). doi: 10.1364/AO.34.002462; pmid: 21052381
79. B. Walther *et al*., Spatial and spectral light shaping with metamaterials. *Adv. Mater.* **24**, 6300–6304 (2012). doi: 10.1002/adma.201202540; pmid: 23065927
80. F. Aieta, M. A. Kats, P. Genevet, F. Capasso, Multiwavelength achromatic metasurfaces by dispersive phase compensation. *Science* **347**, 1342–1345 (2015). doi: 10.1126/science.aaa2494; pmid: 25700175
81. M. Khorasaninejad *et al*., Achromatic metasurface lens at telecommunication wavelengths. *Nano Lett.* **15**, 5358–5362 (2015). doi: 10.1021/acs.nanolett.5b01727; pmid: 26168329
82. J. Cheng, H. Mosallaei, Truly achromatic optical metasurfaces: A filter circuit theory-based design. *J. Opt. Soc. Am. B* **32**, 2115–2121 (2015). doi: 10.1364/JOSAB.32.002115
83. B. Wang *et al*., Visible-frequency dielectric metasurfaces for multiwavelength achromatic and highly dispersive holograms. *Nano Lett.* **16**, 5235–5240 (2016). doi: 10.1021/acs.nanolett.6b02326; pmid: 27398793
84. D. Lin *et al*., Photonic multitasking interleaved Si nanoantenna phased array. *Nano Lett.* **16**, 7671–7676 (2016). doi: 10.1021/acs.nanolett.6b03505; pmid: 27960478
85. W. Zhao *et al*., Full-color hologram using spatial multiplexing of dielectric metasurface. *Opt. Lett.* **41**, 147–150 (2016). doi: 10.1364/OL.41.000147; pmid: 26696180
86. E. Arbabi, A. Arbabi, S. M. Kamali, Y. Horie, A. Faraon, Multiwavelength metasurfaces through spatial multiplexing. *Sci. Rep.* **6**, 32803 (2016). doi: 10.1038/srep32803; pmid: 27597568
87. Z.-L. Deng, S. Zhang, G. P. Wang, Wide-angled off-axis achromatic metasurfaces for visible light. *Opt. Express* **24**, 23118–23128 (2016). doi: 10.1364/OE.24.023118; pmid: 27828377
88. M. Khorasaninejad *et al*., Achromatic metalens over 60 nm bandwidth in the visible and metalens with reverse chromatic dispersion. *Nano Lett.* **17**, 1819–1824 (2017). doi: 10.1021/acs.nanolett.6b05137; pmid: 28125234
89. Y. Li *et al*., Achromatic flat optical components via compensation between structure and material dispersions. *Sci. Rep.* **6**, 19885 (2016). doi: 10.1038/srep19885; pmid: 26794855
90. S. Wang *et al*., Broadband achromatic optical metasurface devices. *Nat. Commun.* **8**, 187 (2017). pmid: 28775300
91. E. Arbabi, A. Arbabi, S. M. Kamali, Y. Horie, A. Faraon, Multiwavelength polarization-insensitive lenses based on dielectric metasurfaces with meta-molecules. *Optica* **3**, 628–633 (2016). doi: 10.1364/OPTICA.3.000628
92. O. Avayu, E. Almeida, Y. Prior, T. Ellenbogen, Composite functional metasurfaces for multispectral achromatic optics. *Nat. Commun.* **8**, 14992 (2017). doi: 10.1038/ncomms14992; pmid: 28378810
93. P. Wang, N. Mohammad, R. Menon, Chromatic-aberration-corrected diffractive lenses for ultra-broadband focusing. *Sci. Rep.* **6**, 21545 (2016). doi: 10.1038/srep21545; pmid: 26868264
94. S. Wang, M. Moharam, R. Magnusson, J. Bagby, Guided-mode resonances in planar dielectric-layer diffraction gratings. *J. Opt. Soc. Am. A* **7**, 1470–1474 (1990). doi: 10.1364/JOSAA.7.001470
95. Z. Lin, B. Groever, F. Capasso, A. W. Rodriguez, M. Lončar, Topology optimized multi-layered meta-optics. arXiv:1706.06715 [physics.optics] (21 June 2017).
96. N. Yu, F. Capasso, Optical metasurfaces and prospect of their applications including fiber optics. *J. Lightwave Technol.* **33**, 2344–2358 (2015). doi: 10.1109/JLT.2015.2404860
97. T. Gissibl, S. Thiele, A. Herkommer, H. Giessen, Two-photon direct laser writing of ultracompact multi-lens objectives. *Nat. Photonics* **10**, 554–560 (2016). doi: 10.1038/nphoton.2016.121

ACKNOWLEDGMENTS

This work was supported in part by the Air Force Office of Scientific Research (grants FA9550-14-1-0389 and FA9550-16-1-015) and by a gift from Huawei Technologies under its HIRP FLAGSHIP program. This work was performed in part at Harvard University's Center for Nanoscale Systems, a member of the National Nanotechnology Coordinated Infrastructure, which is supported by the NSF under award 1541959. We thank W. T. Chen, A. Y. Zhu, Z. Shi, R. C. Devlin, J. Oh, C. Carmes, V. Sanjeev, V. Ding, Y. W. Huang, D. Rousso, I. Mishra, P. Kanhaiya, S. Zhang, A. She, and B. Grover for contributions and useful discussions.

10.1126/science.aam8100

Metalenses: Versatile multifunctional photonic components

Mohammadreza Khorasaninejad and Federico Capasso

Science **358** (6367), eaam8100.
DOI: 10.1126/science.aam8100originally published online October 5, 2017

Looking sharp with metalenses

High-end imaging lenses have tended to be based on bulk optical components. Advances in fabrication techniques have enabled the development of ultrathin, lightweight, and planar lenses (metalenses) that have unprecedented functionalities. These metalenses have the potential to replace or complement their conventional bulk counterparts. Khorasaninejad and Capasso review the evolution of metalenses, summarizing achievements and applications and identifying future challenges and opportunities. Metalenses can have numerous applications, ranging from cellphone camera modules, to wearable displays for augmented and virtual reality and machine vision, to bio-imaging and endoscopy.

Science, this issue p. eaam8100